Journal of Applied Polymer Science

Interaction of Nafion Ionomers Toward Various Solvents

K. S. Santhosh Kumar,[1] K. P. Vijayalakshmi,[2] Sangeetha Sivanath,[2] T. Jayalatha,[2] Surajeet Mohanty,[3] M. Shaneeth[3]

[1]Polymers and Special Chemicals Division, Vikram Sarabhai Space Centre, Thiruvananthapuram 695022, Kerala, India
[2]Analytical and Spectroscopy Division, Vikram Sarabhai Space Centre, Thiruvananthapuram 695022, Kerala, India
[3]Lithium Ion Fuel Cell Division, Vikram Sarabhai Space Centre, Thiruvananthapuram 695022, Kerala, India
Correspondence to: K. S. S. Kumar (E-mail: santhoshkshankar@yahoo.com)

ABSTRACT: Interactions of Nafion (Naf) ionomer with water, aqueous ethanol (EA), aqueous isopropyl alcohol (IPA), and aqueous ammonia were investigated by attenuated total reflectance (ATR)–infrared (IR) spectroscopy, differential scanning calorimetry, thermogravimetric analysis, and computational modeling studies. Microstructural features by ATR–IR revealed the existence of hydrophilic interaction of Naf with all solvents. The Naf membranes formed hydrogen bonds with water, aqueous EA, and IPA. The incorporation of solvents on the Naf matrix impaired the crystallinity, which was highest in the case of IPA. Of all the microsolvated structures of Naf investigated, the formation of H_3O^+ ions was evident; in addition, $H_5O_2^+$ ions appeared in the alcohol–water mixture, and NH_4^+ ions were observed in the water–ammonia mixture along with a direct ion pair with the SO_3^- group in Naf. Theoretical studies based on computational modeling disclosed that the interchain distance increased with enhanced interactions (hydrophobic interactions in particular), and this was in good agreement with the highest swelling ratio of the Naf membrane in aqueous IPA and EA solvents. © 2012 Wiley Periodicals, Inc. J. Appl. Polym. Sci. 128: 3710–3719, 2013

KEYWORDS: membranes; molecular modeling; spectroscopy

Received 20 June 2012; accepted 1 August 2012; published online 10 October 2012
DOI: 10.1002/app.38421

INTRODUCTION

Nafion (Naf) membranes are widely used as proton-conducting membranes in polymer electrolyte membrane fuel cells.[1–3] The high energy efficiency and high power density of polymer electrolyte membrane fuel cells are mainly attributed to the exceptional proton conductivity and mechanical sturdiness of Naf membranes. This membrane belongs to the class of perfluorinated ionomers and is composed of a hydrophobic perfluorocarbon backbone and vinyl ether side chains terminated with hydrophilic sulfonic acid groups. The presence of hydrophobic and hydrophilic groups leads to the nanoscale segregation of the polymer, and this behavior varies dramatically with the properties of the solvent, namely, the polarity, acidity, hydrogen-bonding efficiency, and hydrophobic/hydrophilic interactions with the solvents.[4–11]

The morphology of Naf and Naf–water interaction have been widely investigated with various instrumental techniques, and these studies have revealed the proton conductivity of Naf membranes.[12–17] Depending on the concentration of $-SO_3H$ and the water content, the ionic groups in Naf form clusters in smaller or larger aggregates, which pave route for proton conduction.[18] The high affinity of sulfonic acid groups to water facilitates the dissociation of O—H bonds. Hence, with increasing water content, the proton (H^+) concentration increases and leads to an enhancement in the proton conductivity. Dissociated protons may also interact with water molecules to form hydronium ions (H_3O^+).[19] Although the aforementioned mechanistic interpretations have been proposed for the water-induced enhancement of proton conductivity, a lack of clarity exists as to the actual mechanism of proton transport and the shape and size of the water clusters.[20] Vibrational spectroscopy has furnished quite a bit of evidence for the interactions of water molecules confined in membranes[20,21] with or without fillers.[22,23] The stretching vibrations of the hydroxyl groups have been found to be very sensitive to the local environment of water molecules,[22–25] whereas the structure of the membrane is very sensitive to the presence of even a small quantity of organic solvents.[26,27]

Atomic force microscopy has been used for morphological studies on Naf membranes in the presence of water, water–methanol, water–ethanol (EA), and water–isopropyl alcohol (IPA).[28] Furthermore, small-angle neutron scattering, small-angle X-ray

scattering, and electron spin resonance techniques have been used for the analysis of the structure of Naf molecules in water and aliphatic alcohols. These studies have revealed the aggregated structure of the perfluorocarbon backbone of Naf.[29–34] Dynamic light scattering experiments of Naf and EA–water mixtures (50/50) and Naf and methanol–water mixtures (50/50) have unraveled a defined picture of aggregated structures in Naf. Among the aggregated particles, two different sizes of Naf have been observed; one due to the hydrophobic interaction of the fluorocarbon backbone and the other due to electrostatic interaction of sulfonic acid ion pairs of vinyl ether side chains.[35] Recent studies using the attenuated total reflectance (ATR)–Fourier transform infrared technique[36] have dealt with the hydration aspects of Naf. Recently, detailed analyses of clustering and percolation through atomistic simulation approach have also been reported.[37,38]

In this article, we address in detail the interactions of Naf membranes with various solvents. The selected solvent systems are water, water–EA, water–IPA, and water–ammonia mixtures. EA and IPA are able to show good H-bonding tendencies, whereas their hydrophobic moieties can undergo significant interactions with the perfluorinated backbone. Ammonia has good H-bonding efficiency and also acts as a weak base. In addition, alcohols and ammonia have a significant difference in polarity and H^+ releasing efficiency compared to water. The possibilities of the formation of ions such as H_3O^+, $H_5O_2^+$, and NH_4^+ were discussed in a previous work.[19] However, no strong proof for the formation of these ions was presented. In this study, molecular modeling studies were attempted to obtain clear evidence for the formation of these ions. ATR–IR spectroscopy, differential scanning calorimetry (DSC), thermogravimetric analysis (TGA), and computational modeling were used to collect evidence of the interactions of the Naf membranes with these solvents.

EXPERIMENTAL

Materials

Naf 117 membranes (molecular weight = 1100 g/equiv and thickness = 5 mil or 127 μm, Nafion (DuPont, USA)) were used for the study. Deionized water (MilliQ), EA (99.9%, SDFCL, Mumbai, India), IPA (99.5%, Fischer, Mumbai, India), and an extrapure ammonia solution (25%, SDFCL, Mumbai, India) were used as received.

Methods

Sample Preparation. The Naf membranes were cut into small pieces and boiled for 1 h in 1*M* H_2SO_4. The samples were taken out, the surfaces were wiped, and the membranes were dipped in water and various aqueous solvents (25% v/v) for 1 h. A dipping time of 1 h was chosen for comparative purposes and to support modeling studies (*vide infra*). The swelling percentages (area wise) of the membranes in different aqueous solvents were measured. These samples were then subjected to ATR–IR spectroscopy, DSC, and TGA.

Characterization. The ATR–IR spectra of the membranes were measured with a PerkinElmer spectrum GXA Fourier transform infrared spectrometer equipped with a diamond ATR accessory (Perkin Elmer, USA). The spectra were recorded in the wavenumber range 4000–550 cm^{-1} at a resolution of 4 cm^{-1}. Each membrane treated with the solvents was squeezed between the surface of a diamond crystal and a pressing device to obtain perfect contact. DSC experiments of the membranes were performed with a DSC 2920 thermal analysis instrument (TA instruments, USA). About 20 mg of sample was used for the analysis. The surface of each sample was wiped with lens paper to remove solvent from the surface of the membrane. The analyses were carried out at a heating rate of 10°C/min up to a temperature of 300°C. TGA studies of the membranes were performed under air with a simultaneous thermogravimetry–differential thermal analysis 2960 instrument (TA instruments, USA). The thermograms were recorded up to 600°C at a heating rate of 10°C/min. Swelling studies were carried out through immersion of Naf films in aqueous solvents for 1 h, and the swelling ratios (area wise) were calculated.

Molecular modeling studies have been conducted with the semiempirical PM6 method,[39,40] as implemented in the Gaussian 09 suite of programs.[41] PM6 uses experimental and *ab initio* data from over 9000 compounds, covering 80 elements, and is arguably the best semiempirical method to date. It has shown good performance in modeling for a wide range of problems. The equivalent weight of the Naf membrane used for our experimental studies was 1100 g/mol, and to approximately match this number, we modeled a copolymer model of Naf by selecting a tetrafluoroethylene backbone consisting of 14 carbon atoms in which the second carbon atom was bonded to the sulfonic acid group terminated perfluorovinyl ether group. The molecular formula of the modeled system was $C_{19}F_{49}O_5SH$. To incorporate intermolecular interaction, two such copolymer systems were used. All of the structures were optimized *in vacuo* and in water, the water–EA mixture, the water–IPA mixture, and the water–ammonia mixture. To incorporate the solvation effects, a microsolvation approach with explicit solvent molecules was used.

RESULTS AND DISCUSSION

ATR–IR Analysis

Figure 1(a) represents the complete ATR–IR spectra of Naf membranes recorded in different solvents. Major differences were seen in the —OH stretching vibration (3300–3500 cm^{-1}) and bending vibration bands at 1657 cm^{-1} (marked regions). The bands between 557 and 674 cm^{-1} were attributed to the —CF_2 (hydrophobic region) vibrations, such as torsion, wagging, and rocking [Figure 1(b)]. This region of the IR spectra did not show any significant change in the presence of various solvents. The band at 805 cm^{-1} is attributed to —C—S stretching (hydrophilic region), which underwent some changes in the presence of alcohols. For instance, in EA, it became broad and less intense, whereas in IPA, it shifted to 815 cm^{-1}. These observations suggest that the hydrophilic interactions were more dominant than the hydrophobic interactions. The band at 877 cm^{-1} observed in the water–alcohol mixtures were assigned to the —C—H— stretching of the solvent. The peaks at 970 and 981 cm^{-1} were due to —C—O—C stretching vibrations, which remained almost unchanged with different solvents. Meanwhile, IPA showed an additional band at 948 cm^{-1} [Figure 1(c)]. This band may be due to the change in —C—O—C stretching due to the greater penetration of IPA into the Naf.

Applied Polymer SCIENCE

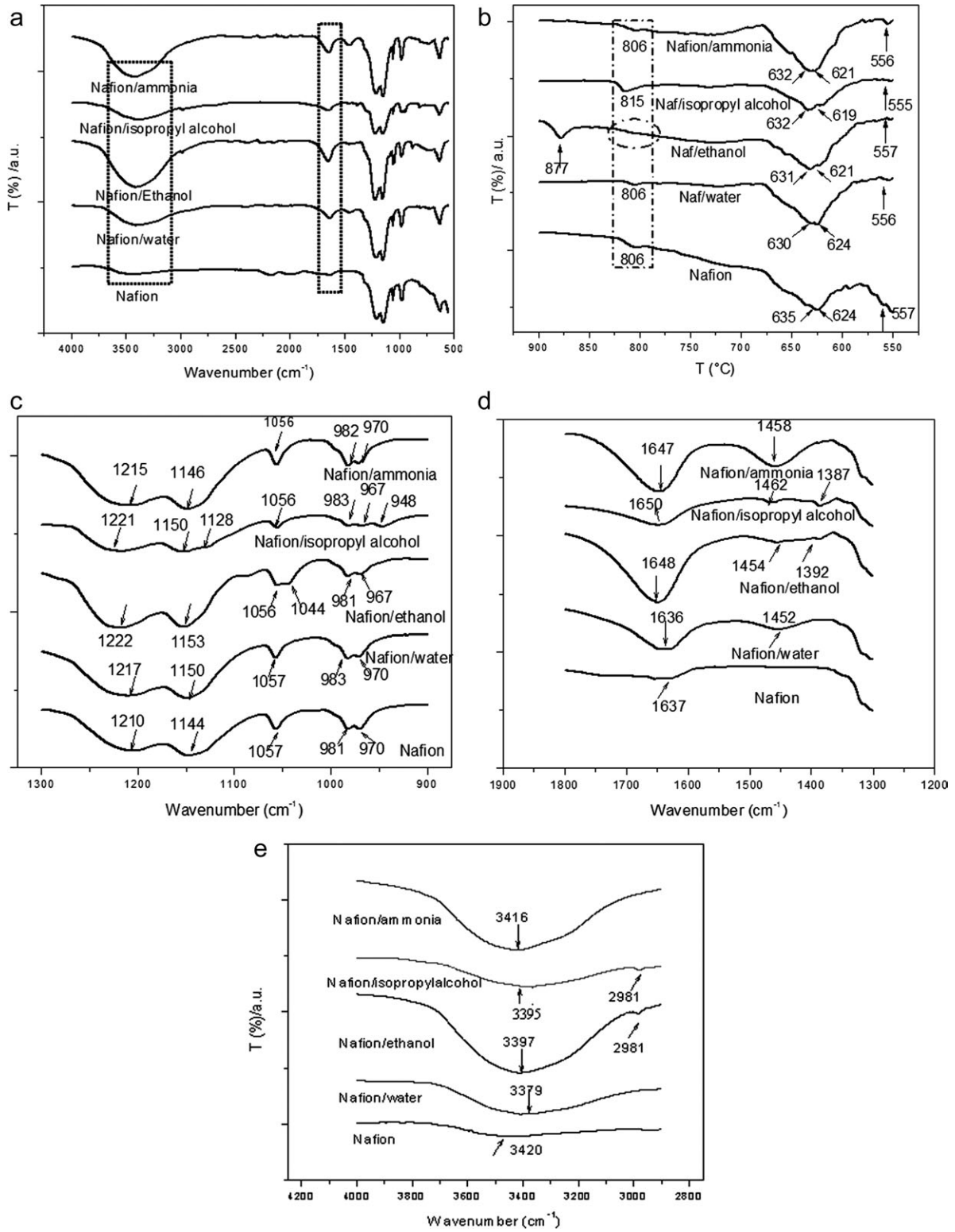

Figure 1. ATR–IR spectra of Naf in water and aqueous solvents (a) complete spectra (4000–500 cm^{-1}), (b) region between 850 and 550 cm^{-1}, (c) region between 1300 and 900 cm^{-1}, (d) region between 1800 and 1300 cm^{-1}, and (e) region between 4000 and 2900 cm^{-1}.

The hydrophobic parts of EA and IPA were expected to interact with the polytetrafluoroethylene backbone and lead to a change in the —CF_2 bands. However, no significant changes in the —CF_2 bands were observed, even in an alcohol environment, as the hydrophobic interactions were too weak to cause any noticeable changes. However, the —CF_2 stretching vibration peaks [Figure 1(c)] shifted slightly from 1210 cm^{-1} (untreated Naf) to 1217 cm^{-1} (water), 1222 cm^{-1} (EA), 1221 cm^{-1} (IPA), and

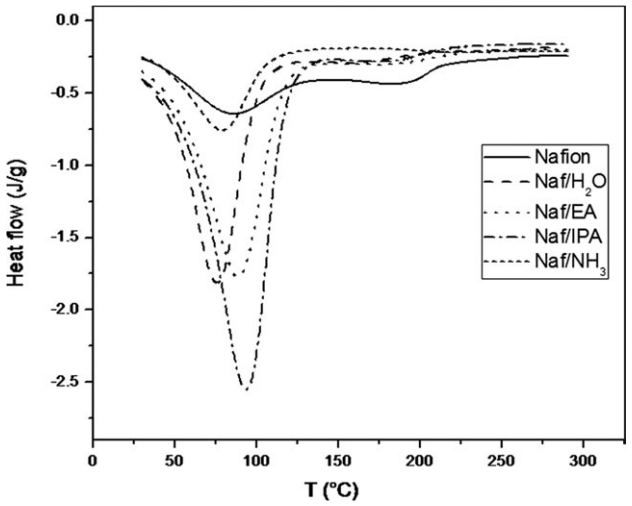

Figure 2. DSC thermograms of the pristine and solvent-treated Naf membranes.

1215 cm^{-1} (ammonia), respectively. These shifts in EA and IPA indicated that interactions toward the fluorinated backbone also existed, along with hydrophilic interactions. In the case of aqueous ammonia treated membranes, no noticeable shift in this peak was observed. At the same time, hydrophobic interactions of Naf to alcohols were revealed in the swelling experiment (*vide infra*).

Stretching vibrations of —S(O)—O were not observed clearly in pristine Naf, whereas they were observed at 1452, 1454, 1462, and 1458 cm^{-1} in membranes treated with water, aqueous EA, aqueous IPA, and ammonia, respectively [Figure 1(d)]. An additional peak was also observed at 1392 and 1387 cm^{-1} in the case of the EA- and IPA-treated membranes; this implied the extensive coordination of alcohol to the —SO_3H groups. The peaks newly emerged at 1637, 1636, 1648, 1650, and 1647 cm^{-1} in pristine Naf, water, aqueous EA, aqueous IPA, and aqueous ammonia treated Naf, respectively, were due to the stretching of hydrated

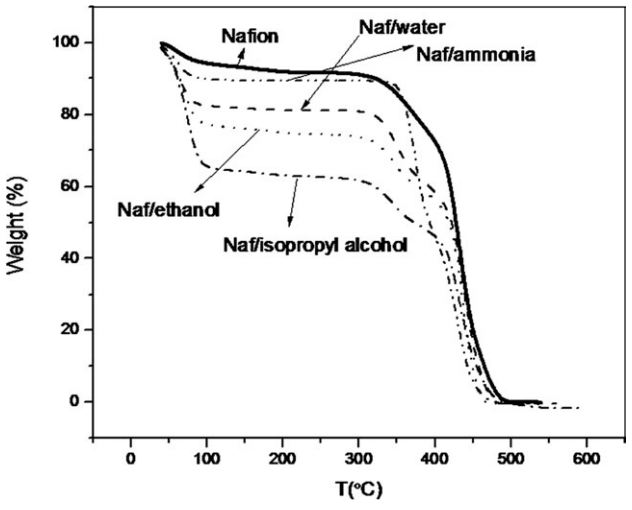

Figure 3. Thermogravimetric spectra of the untreated membrane and membranes in the presence of solvents.

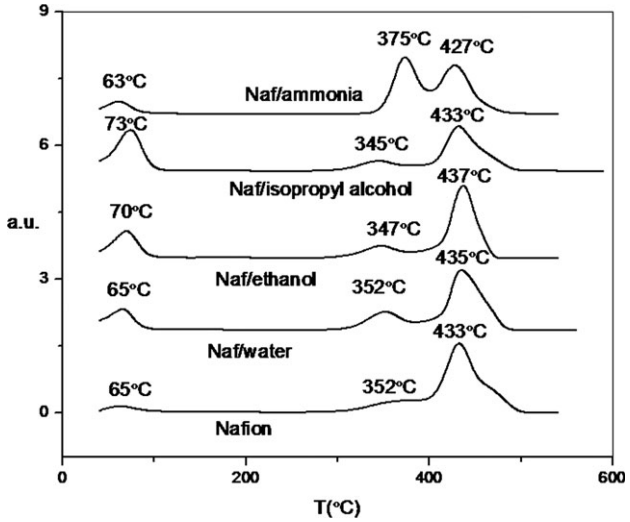

Figure 4. Derivative thermograms of the Naf membranes in different solvents.

protons. The highest intensity of the hydronium ion band was observed for EA, and only a very less intense band was observed for pristine Naf; this might have arisen from interaction with atmospheric moisture. This experimental observation of hydronium ion formation was further supported by the theoretically calculated IR spectra of the corresponding membranes (cf.SI).

Figure 1(e) shows the ATR–IR spectra of all of the treated membranes in the 2800–4200-cm^{-1} frequency range. The Naf membrane without any solvent exhibited only one broad and a very less intense band at 3420 cm^{-1}. This low intensity indicated the absence of —OH groups on the membrane surface. When treated with water, the broad band became more intense and decreased to 3379 cm^{-1}; this suggested the existence of strong hydrogen bonding in the Naf membrane in the presence of water. Meanwhile, with water–EA and water–IPA, the peak shifted to 3397 and 3390 cm^{-1}, respectively; this implied a considerable amount of hydrogen bonding. Ammonia, being a base, prefers to abstract H^+ from the —SO_3H moiety rather than form H bonds. The formation of NH_4^+ was further exposed in molecular modeling studies (*vide infra*).

Thermal Studies

The DSC profiles of the Naf membranes in different solvents are shown in Figure 2. All Naf samples exhibited two endothermic peaks. The first peak corresponded to the evaporation/vaporization of solvent confined in the membrane during treatment.[1–3] The heats of enthalpy of these transitions were 90, 304, 351, 523, and 131 J/g for pristine Naf, Naf/water, Naf/EA, Naf/IPA, and Naf/ammonia, respectively. It was implied that EA and IPA promoted swelling; this was reflected in the heat of reaction (ΔH) increase in those membranes. A high degree of swelling of the membranes in IPA implied the penetration of solvent into polymer chain due to favorable hydrophobic interactions. The Naf–ammonia membranes showed a first transition similar to that of the untreated Naf, as ammonia could not penetrate the Naf matrix effectively.

Table I. Decomposition Characteristics of the Solvent-Treated Naf Membranes

	Decomposition stage					
	First stage		Second stage		Third stage	
Sample	T_{max} (°C)	Weight loss (%)	T_{max} (°C)	Weight loss (%)	T_{max} (°C)	Weight loss (%)
Untreated Naf	65	3	352	15	433	52
Naf-water	65	11	352	29	435	64
Naf-EA	70	11	347	34	437	63
Naf-IPA	73	13	345	45	433	73
Naf-ammonia	63	7	375	22	427	73

T stands for temperature.

The second endotherm was assigned to the melting of crystalline domains. The melting point of the crystalline fluoropolymer backbone occurred at 190°C in pristine Naf. The treated Naf membranes exhibited this endotherm at a low temperature of about 160°C. The entrapped solvents disturbed the crystallinity of the polytetrafluoroethylene structure, which resulted in the fast melting of membranes. These changes were attributed to the hydrophilic/hydrophobic interactions of solvents, which eventually increased the interchain difference in Naf.

Figure 3 shows the thermograms of the pristine and treated Naf membranes. The Naf membranes underwent a three-stage decomposition processes, as shown in the thermograms. The first stage was due to the evaporation of the solvent. The second and third stages were attributed to desulfonation and main-chain degradation, respectively. Derivative TGA provides the rate of these degradation processes (Figure 4). All degradation peaks were almost in the same temperature range for all the samples, except the second peak in the Naf /ammonia membrane. This was ascribed to the ion-pair-complex formation between ammonia and —SO_3H groups, which may have hindered the early decomposition of the sulfonic acid moiety. It was interesting that the desulfonation processes were slower compared to the main degradation. The peak temperature of decomposition (T_{max}) and weight loss at each decomposition stages are collected in Table I.

Molecular Modeling Studies

The optimized structures of the Naf single chain and double chain are presented in Figure 5. In the double-chain structure, no significant attractive interactions were present, as the highly fluorinated alkyl chains in the Naf backbones were repelled because of lone pair–lone pair interactions from fluorine atoms. These interactions did not allow the close proximity of polar sulfonic acid moieties. Also, we noted that the percentage of —SO_3H/chain was very low compared to the fluorinated alkyl chain. The bond length features of the sulfonic acid moiety were nearly unchanged compared to the single chain. The average values of C—F, C—C, and C—O bond distances were 1.34, 1.57, and 1.40 Å, respectively, in both cases.

The solvated structures of Naf single chains in the water (nine water molecules), water–EA (nine water and two EA molecules), water–IPA (seven water and two IPA molecules), and water–ammonia (seven water and two ammonia molecules) mixtures are presented in Figure 6. The O—H bond of the sulfonic acid group was dissociated, and the released proton formed hydronium ions in the case of the water, water–EA mixture, and water–IPA mixture. On the other hand, in the presence of ammonia, ammonium ions were formed. Naf in the water–ammonia mixture showed relatively weaker hydrogen bonds (typically in the range of 1.90–2.10 Å) than those in all of the other systems (typically in the range of 1.55–1.75 Å). The

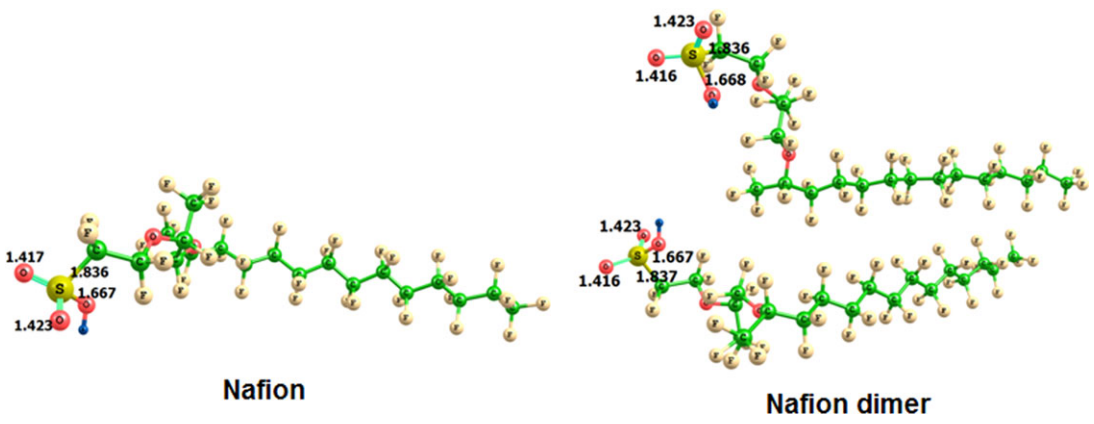

Figure 5. Optimized structures of the Naf and Naf dimer. Bond lengths in angstroms are shown for the bonds around the sulfur atom. [Color figure can be viewed in the online issue, which is available at wileyonlinelibrary.com.]

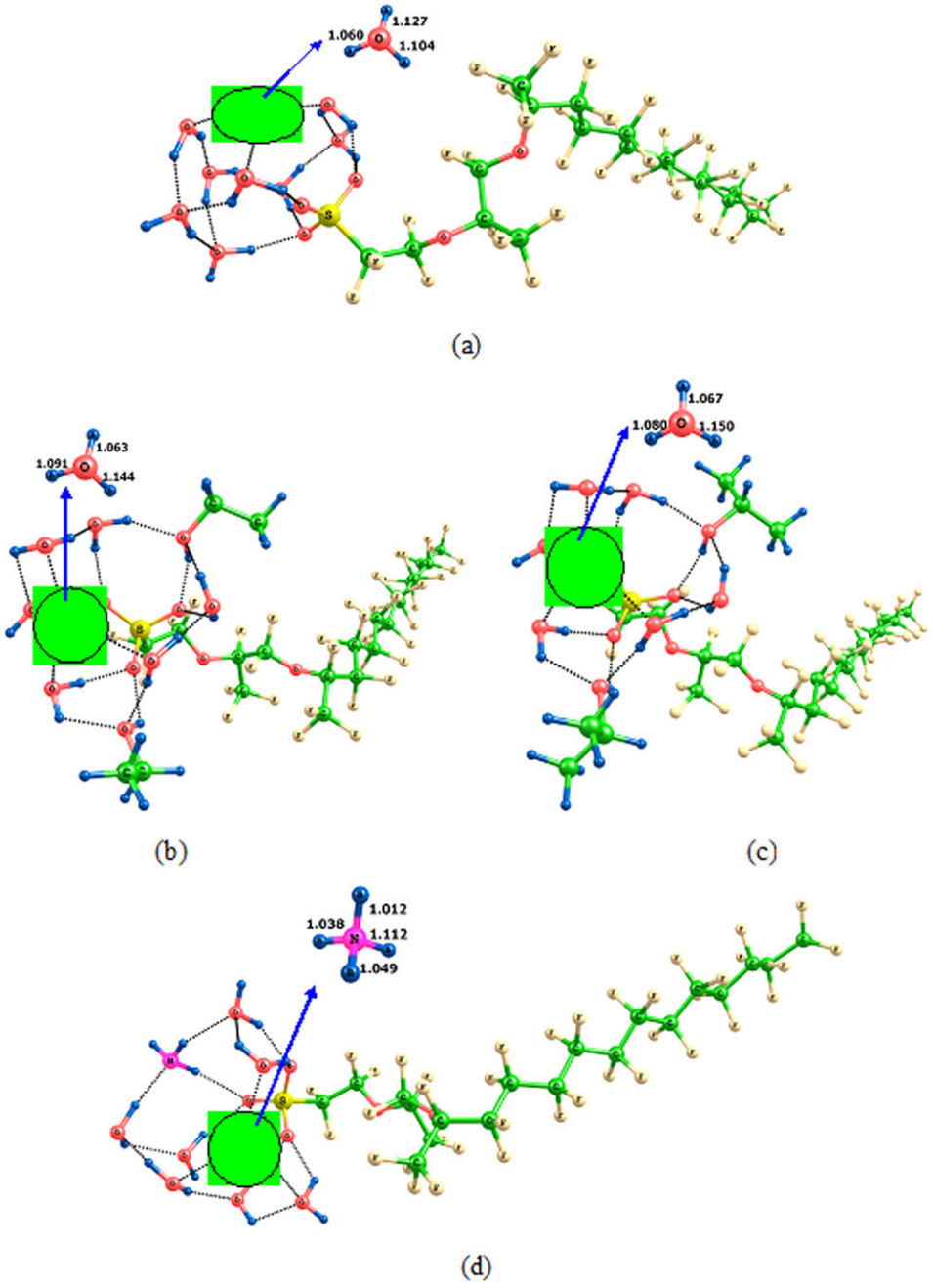

Figure 6. Solvated Naf structures. The ions marked inside the transparent circles are noted separately with blue arrows (all distances are in angstroms). [Color figure can be viewed in the online issue, which is available at wileyonlinelibrary.com.]

release of protons from the ammonium ion may be more difficult than that from hydronium ions as the former is involved in weaker hydrogen bonds than the latter. The experimentally measured hike in desulfonization temperature in TGA might have been due to the strong ionic bonds formed between the ammonium ions and SO_3^- groups compared to the weak hydrogen bonds formed between the latter with all of the other solvents.

The IR stretching frequencies of all of the solvated systems were calculated (see the Supporting Information). In all cases, sharp new peaks appeared in the range 1760–1850 cm^{-1}, and a broadening of the higher wave-number peaks around 2200–2800 cm^{-1} was observed. The higher wave-number peaks were assigned to the stretching of the solvent molecules, whereas the new sharp peaks in the range 1760–1850 cm^{-1} corresponded to the stretching of the hydronium/ammonium ions. In Figure 1(a) (experimental IR spectra), the appearance of a new peak around 1650 cm^{-1} was correlated with the new sharp peak observed in the calculation. In the experiment, the hydronium/ammonium ions were in the dynamic state as the proton underwent a hopping mechanism. This hopping mechanism decreased the overall strength of the corresponding O—H and N—H vibrations, and thus, a decrease in the stretching frequency compared to the actual calculated value was expected.

Applied Polymer SCIENCE

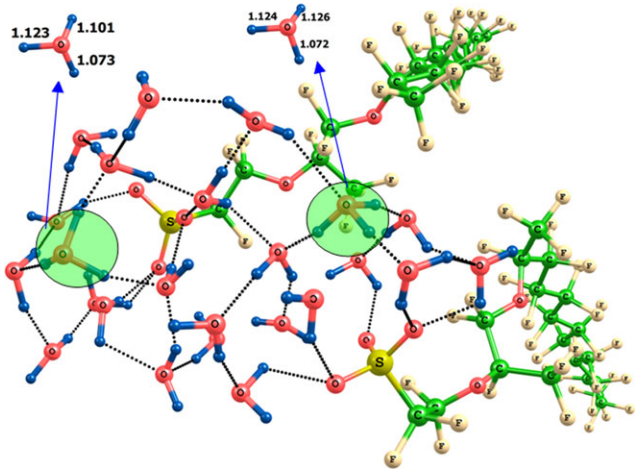

Figure 7. Optimized structure of two polymer chains of Naf in the presence of a microsolvation environment provided by 24 water molecules. All distances are in angstroms. [Color figure can be viewed in the online issue, which is available at wileyonlinelibrary.com.]

Thus, the theoretical results strongly indicated that the appearance of the new peak around 1650 cm^{-1} was due to the formation of loosely bound protons in the solvent.

Further insights into the solvation effects were obtained through the modeling of the double-chain structures (Figures 7–10). Optimized structures of the two polymer chains of Naf in the presence of a microsolvation environment provided by 24 water molecules are shown in Figure 7. With the use of nine water molecules, a good coverage of the sulfonic acid group (all of the S—O bonds were connected to water molecules) of the single chain was obtained. However, with 18 water molecules, full coverage of the hydrophilic portion of the dimer system was not possible. Additional water molecules were necessary to fill some of the void space between the two sulfonic acid groups, and full coverage was achieved with 24 water molecules (12 per chain). The ratio of solvent to water was nearly identical to the experimental condition of 25% v/v both in the single-chain and double-chain models.

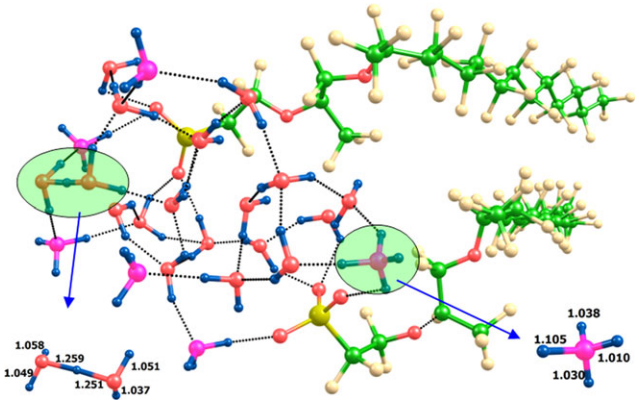

Figure 10. Optimized structure of two polymer chains of Naf in the presence of a microsolvation environment provided by 18 water molecules and six ammonia molecules. All distances are in angstroms. [Color figure can be viewed in the online issue, which is available at wileyonlinelibrary.com.]

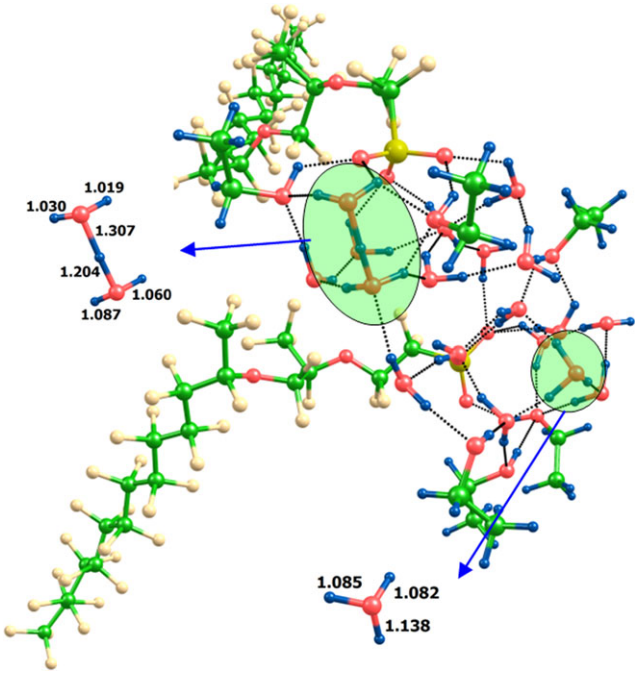

Figure 8. Optimized structure of two polymer chains of Naf in the presence of a microsolvation environment provided by 18 water molecules and six EA molecules. All distances are in angstroms. [Color figure can be viewed in the online issue, which is available at wileyonlinelibrary.com.]

The proton from each sulfonic acid group was transferred to nearby water molecules to form two hydronium ions. The two hydronium ions are marked inside transparent circles and are also noted separately with arrows in the figures. Furthermore,

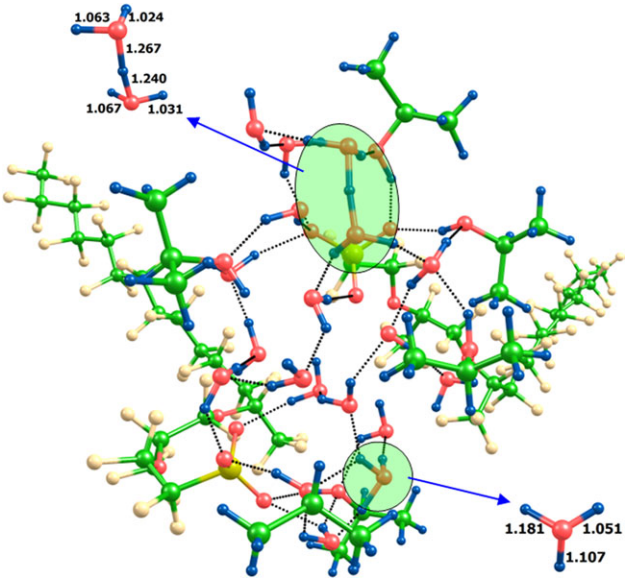

Figure 9. Optimized structure of two polymer chains in the presence of a microsolvation environment provided by 18 water molecules and six IPA molecules. All distances are in angstroms. [Color figure can be viewed in the online issue, which is available at wileyonlinelibrary.com.]

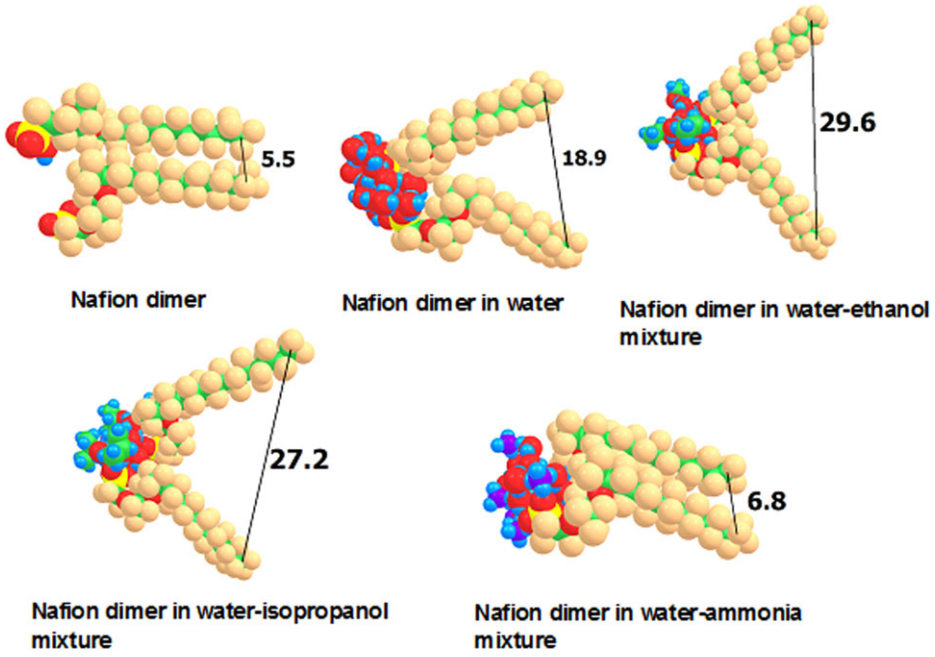

Figure 11. Space-filling model of the Naf dimer *in vacuo* and in solvents. The distance between the terminal carbon atoms are given in angstroms. [Color figure can be viewed in the online issue, which is available at wileyonlinelibrary.com.]

the optimized structure of the two polymer chains of Naf in the presence of a microsolvation environment provided by 18 water molecules and 6 EA molecules is shown in Figure 8. The proton from each of the sulfonic acid groups was transferred to nearby water molecules to form a hydronium ion and an $H_5O_2^+$ ion. The ions are marked inside transparent circles and are also noted separately with blue arrows. The optimized structure of the two polymer chains in the presence of a microsolvation environment provided by 18 water molecules and 6 IPA molecules are shown in Figure 9. The proton from each of the sulfonic acid group was transferred to nearby water molecules to form a hydronium ion and an $H_5O_2^+$ ion. The ions are marked inside transparent circles and are also noted separately with arrows.

Figure 10 represents the optimized structure of two polymer chains of Naf in the presence of a microsolvation environment provided by 18 water molecules and 6 ammonia molecules. Protons from each of the sulfonic acid groups were transferred to nearby water molecules and ammonia molecules to form $H_5O_2^+$ ions and NH_4^+ ions. The ions are marked inside transparent circles and are also noted separately with arrows. All distances are given in angstroms. In the case of the double-chain structure in water, two hydronium ions were formed. Hydronium ions were formed along with $H_5O_2^+$ ions in the cases of both the water–EA and water–IPA Naf membranes. In the case of the water–ammonia mixture, ammonium ions were formed along with the $H_5O_2^+$ ions. Consequently, Naf in the water–ammonia system showed weaker hydrogen bonding than the rest. In Figure 11, the space-filling models of the dimer systems are depicted. As shown, Naf *in vacuo* and also in the water–ammonia mixture showed the most compact arrangement. In water, the hydrophobic region was expanded to some extent, whereas this expansion was substantial in the case of both the water–EA and water–IPA mixtures. The interchain distances increased up to 30 Å in the presence of alcohols. The experimental swelling ratio of Naf in various solvents decreased in the following order: IPA (90%) > EA (87%) > Water (18%) > Ammonia (<2%); this corroborated the computational study. The difference observed in interchain distance was proportional to the swelling and is tabulated in Table II. The high swellability of the membranes in EA and IPA originated from preferential hydrophobic interaction with the Naf backbone. According to the theoretical calculations, membranes in the water–EA mixture were expected to be more swollen than those in the water–IPA mixture, but experimentally, this was flipped over, even though the difference was minimal.

Table II. Swelling (Experimental) and Interchain Distance (from Modeling) of the Naf Membranes in Different Solvents

Solvent	Swelling (%; experimental)	Interchain distance (modeling)
Water	18	18.9
Aqueous EA	87	29.6
Aqueous IPA	90	27.2
Aqueous ammonia	2	6.8

These theoretical studies indicate that in all of the cases, the sulfonic acid moiety was the major interaction site for the solvent. Solvent molecules aggregated around the hydrophilic sulfonic acid groups. Solvation led to the dissociation of the O—H bond of the sulfonic acid group. The released proton was

accommodated by water to form either a hydronium ion or a $H_5O_2^+$ ion. The presence of ammonia retarded the formation of water–bound ions and instead promoted the formation of ammonium ions. The presence of ammonia also weakened the overall hydrogen-bonding interactions in the system. The hydrophobic interactions between the Naf backbone and absorbed solvent molecules were expected to be much weaker than the hydrophilic interactions. These results also support the existence of an exchange of protons from one water molecule to others through a hydrogen-bonding network (hydrogen bonding was also noted in the ATR–IR study), and this suggested the possibility of a dynamic mechanism of proton transport.

CONCLUSIONS

The interactions of various solvents with Naf membranes were investigated. The solvents, water, aqueous EA, and aqueous IPA, were able to build strong hydrogen bonds with the —SO_3H moieties in the Naf ionomers. A detailed study with ATR spectroscopy was performed to unfold the microstructural features of the Naf membranes in the presence of solvents. EA and IPA showed notable hydrophilic and hydrophobic interactions with Naf. Molecular modeling studies suggested the existence of ionic clusters in the presence of water. The formation of hydronium ions (in all of the solvents studied), $H_5O_2^+$ ions (in the alcohol–water mixture), and NH_4^+ ions (in the water–ammonia mixture) were confirmed by theoretical studies. In the latter case, ammonium ions formed a direct ion pair with the SO_3^- group in Naf, as indicated in the theoretical studies. These insights will enhance the robustness of electrode processing steps and, in turn, help to achieve improved performance in Naf membranes in fuel cells.

ACKNOWLEDGMENTS

The authors acknowledge the director, vikram sarabhai space centre (VSSC), for granting them permission to publish this article. The analytical support provided by the Analytical and Spectroscopy Division of VSSC is also gratefully acknowledged. The authors also thank C. P. Reghunadhan Nair for valuable corrections to the article.

REFERENCES

1. Chen, C.; Levitin, G.; Hess, D. W.; Fuller, T. F. *J. Power Sources* **2007**, *169*, 288.
2. Li, T.; Wlaschin, A.; Balbuena, P. B. *Ind. Eng. Chem. Res.* **2001**, *40*, 4789.
3. Tang, H.; Peikang, S.; Jiang, S. P.; Wang, F.; Pan, M. *J. Power Sources* **2007**, *170*, 85.
4. Haubold, H. G.; Vad, T.; Jungbluth, H.; Hiller, P. *Electrochim. Acta* **2001**, *46*, 1559.
5. Saarinen, V.; Kruer, K. D.; Schuster, M.; Merkle, R.; Maier, J. *Solid State Ionics* **2007**, *178*, 533.
6. Chaabane, L.; Dammak, L.; Nikonenko, V. V.; Bulvestre, G.; Auclair, B. *J. Membr. Sci.* **2007**, *298*, 126.
7. Berezana, N. P.; Akononenko, N.; Dyomina, O. A.; Gnusina, N. P. *Adv. Colloid Interface Sci.* **2008**, *139*, 3.
8. Kawamura, J.; Hattori, K.; Hongo, T.; Asayama, R.; Kuwata, N.; Hattori, T.; Mizusaki, J. *Solid State Ionics* **2005**, *176*, 2451.
9. Heitner-Wirguin, C. *J. Membr. Sci.* **1996**, *120*, 1.
10. Grot, W. G. *Macromol. Symp.* **1994**, *82*, 161.
11. Doyle, M.; Rajendran, G. In Handbook of Fuel Cells-Fundamentals, Technology and Applications; Perfluorinated Membranes; Wiley: Hoboken, NJ, **2010**.
12. Tovbin, Y. K.; Vasyatkin, N. F. *Colloids Surf. A* **1999**, *158*, 385.
13. Goering, R. M.; Bowman, C. N.; Koval, C. A.; Noble, R. D.; Williamson, D. L. *J. Membr. Sci.* **1998**, *144*, 133.
14. Li, J. Y.; Nemat-Nasser, S. *Mech. Mater.* **2000**, *32*, 303.
15. Gebel, G. *Polymer* **2000**, *41*, 5829.
16. Rollet, A. L.; Diat, O.; Gebel, G. *J. Phys. Chem. B* **2002**, *106*, 3033.
17. Kim, M. H.; Glinka, C. J.; Grot, S. A.; Grot, W. G. *Macromolecules* **2006**, *39*, 4775.
18. Yeo, S.; Eisenberg, A. *J. Appl. Polym. Sci.* **1977**, *21*, 875.
19. Zecchina, A.; Geobadlo, F.; Poto, G. S.; Bordiga, S.; Ricchiardi, G.; Buzzoni, R.; Petrini, G. *J. Phys. Chem.* **1995**, *99*, 11937.
20. Elliot, J. A.; Hanna, S.; Elliot, A. M. S.; Cooley, G. *Phys. Chem. Chem. Phys.* **1999**, *1*, 4855.
21. Bribes, J. L.; Elboukari, M.; Maillols, J. *J. Raman Spectrosc.* **1991**, *22*, 275.
22. Di Noto, V.; Gliubizzi, R.; Negro, E.; Vittadello, M.; Pace, G. *Electrochim. Acta* **2007**, *53*, 1618.
23. Di Noto, V.; Piga, M.; Piga, L.; Polizzi, S.; Negro, E. *J. Power Sources* **2008**, *2*, 561.
24. Ostrovskii, D. I.; Torell, L. M.; Paronen, M.; Hietala, S.; Sundholm, F. *Solid State Ionics* **1997**, *7*, 315.
25. Hietala, S.; Holmberg, S.; Nasman, J.; Ostrovskii, D.; Paronen, M.; Serimaa, R.; Sundholm, F.; Torell, L.; Torkkeli, M. *Angew. Makromol. Chem.* **1996**, *243*, 151.
26. Chaabane, L.; Bulvestre, G.; Innocent, C.; Pourcelly, G.; Auclair, B. *Eur. Polym. J.* **2006**, *42*, 1403.
27. Neburchilov, V.; Martin, J.; Wang, H.; Zhang, J. *J. Power Sources* **2007**, *169*, 221.
28. Affoune, A. M.; Yamada, A.; Umeda, M. *J. Power Sources* **2005**, *148*, 9.
29. Aldebert, P., Gebel, G., Loppinet, B.; Nakamura, N. *Polymer* **1995**, *36*, 431.
30. Aldebert, P.; Dreyfus, B.; Pineri, M. *Macromolecules* **1986**, *19*, 2651.
31. Loppinet, B.; Gebel, G.; Williams, C. E. *J. Phys. Chem. B* **1997**, 101, 1884.
32. Szajdzinska-Pietek, E.; Schlick, S. *Langmuir* **1994**, *10*, 1101.
33. Szajdzinska-Pietek, E.; Schlick, S. *Langmuir* **1994**, *10*, 2188.
34. Li, H.; Schlick, S. *Polymer* **1995**, *36*, 1141.
35. Cirkel, P. A.; Okada, T.; Kinugasa, S. *Macromolecules* **1999**, *32*, 531.
36. Kunimatsu, K.; Bae, B.; Miyatake, K.; Uchida, H.; Watanabe, M. *J. Phys. Chem. B* **2011**, *115*, 4315.

37. Idupulapati, N.; Devanathan, R.; Dupuis, M. *J. Phys. Chem. B* **2011**, *115*, 2959.

38. Devanathan, R.; Venkatnathan, A.; Rousseau, R.; Dupuis, M.; Frigato, T.; Gu, W.; Helms, V. *J. Phys. Chem. B* **2010**, *114*, 13681.

39. Stewart, J. J. P. *J. Mol. Model.* **2007**, *13*, 1173.

40. Stewart, J. J. P. MOPAC2009; Stewart Computational Chemistry: Colorado Springs, CO, **2008**.

41. Frisch, M. J.; Trucks, G. W.; Schlegel, H. B.; Scuseria, G. E.; Robb, M. A.; Cheeseman, J. R.; Scalmani, G.; Barone, V.; Mennucci, B.; Petersson, G. A.; Nakatsuji, H.; Caricato, M.; Li, X.; Hratchian, H. P.; Izmaylov, A. F.; Bloino, J.; Zheng, G.; Sonnenberg, J. L.; Hada, M.; Ehara, M.; Toyota, K.; Fukuda, R.; Hasegawa, J.; Ishida, M.; Nakajima, T.; Honda, Y.; Kitao, O.; Nakai, H.; Vreven, T.; Montgomery, J. A., Jr.; Peralta, J. E.; Ogliaro, F.; Bearpark, M.; Heyd, J. J.; Brothers, E.; Kudin, K. N.; Staroverov, V. N.; Kobayashi, R.; Normand, J.; Raghavachari, K.; Rendell, A.; Burant, J. C.; Iyengar, S. S.; Tomasi, J.; Cossi, M.; Rega, N.; Millam, J. M.; Klene, M.; Knox, J. E.; Cross, J. B.; Bakken, V.; Adamo, C.; Jaramillo, J.; Gomperts, R.; Stratmann, R. E.; Yazyev, O.; Austin, A. J.; Cammi, R.; Pomelli, C.; Ochterski, J. W.; Martin, R. L.; Morokuma, K.; Zakrzewski, V. G.; Voth, G. A.; Salvador, P.; Dannenberg, J. J.; Dapprich, S.; Daniels, A. D., Farkas, Ö.; Foresman, J. B.; Ortiz, J. V.; Cioslowski, J.; Fox, D. J. Gaussian∼09 Revision; Gaussian: Wallingford CT, **2009**.